RESEARCH ARTICLE

Experimental analysis of the precessing vortex core in a free swirling jet

Fulvio Martinelli · Andrea Olivani · Aldo Coghe

Abstract An experimental analysis of the precessing vortex core (PVC) instability in a free swirling jet of air at ambient pressure and temperature is performed by means of laser Doppler velocimetry (LDV) and particle image velocimetry (PIV). Two parametric studies are considered, varying the swirl parameter and the Reynolds number. The range of parameters considered allowed to study conditions of strong precession as well as the inception and settlement of the instability. Mean velocity and standard deviation profiles, power spectral density functions and probability density functions for the axial and tangential velocity components are presented. Average as well as instantaneous PIV maps are considered in the characterization of the flowfield structure and detection of the instantaneous position of the vortex center. Joint analysis of velocity PDFs and power spectra shows that the PVC contribution to the global statistics of the velocity field can be properly separated from the contribution of the true flow turbulence, giving additional insight to the physics of the precession phenomenon. The results obtained in the explored range of conditions indicate that the true turbulence intensity is not dependent on the swirl parameter.

F. Martinelli (✉)
Dipartimento di Ingegneria Aerospaziale,
Politecnico di Milano, Via La Masa, 34,
Milano 20158, Italy
e-mail: fulvio.martinelli@polimi.it

A. Olivani · A. Coghe
Dipartimento di Energetica, Politecnico di Milano,
Via La Masa, 34, Milano 20158, Italy

1 Introduction

High Reynolds number flows, characterized by high turbulence intensity, recirculation zones and strong unsteadiness, are frequently used in technical applications. Among these flows, strongly swirling ones represent a very important category; they are widely used in cyclone separators and even in combustion processes, in order to enhance reactants mixing and flame stability thus reducing pollutant emissions. Improvement in these technical applications requires a deeper understanding of the dynamics of swirling flows, whose features are still debated by the scientific community.

In particular, the vortex breakdown phenomenon is far from being completely understood in all its features, one of them being the so-called precessing vortex core (PVC). The PVC occurs in high Reynolds and swirl number flows, and is characterized by the regular precession of the large-scale vortical structure typical of swirling jets around the geometrical axis of symmetry. It is known that the precessing frequency varies linearly with the Reynolds number, at a given swirl intensity.

The study of the instability of strongly swirling flows, mainly confined in tubes, was considered by many authors in the last decades; Sarpkaya (1971) studied experimentally the vortex breakdown, introducing the definition of double helix, spiral, and axisymmetric breakdown. Harvey (1962) defined the breakdown phenomenon as the critical stage between the existence or not of an axial recirculation zone. Interesting visual observations by Chanaud (1965) confirmed the presence of a periodic motion in certain conditions of a swirling flowfield. One of the first works concerning vortex precession in incompressible swirling flows is the one from Cassidy and Falvey (1970), in which the linear dependence of the precessing

frequency on the flowrate is introduced. Novak and Sarpkaya (2000) studied extensively the vortex breakdown phenomenon for high Reynolds number flows in tubes, providing velocity profiles and turbulence data in relevant situations. A model of precessing vortex core was proposed by Wunenburger et al. (1999). Garg and Leibovich (1979) and Akhmetov et al. (2004) studied with laser Doppler velocimetry (LDV) the phenomenon of precession. In Dellenback et al. (1988), the experimental evidence of vortex precession in a direction opposite to the swirl direction is first presented; in the work by Billant et al. (1998) four different forms of vortex breakdown in a swirling water jet are studied, and a novel cone breakdown is presented. Combined use of LDV and PIV in unsteady swirling flows was explored by Grosjean et al. (1997) to capture the unsteadiness of vortex precession; finally, in the recent paper by Cala et al. (2006) significant results of phase-locked LDV measurements in a swirling jet are reported. There is a wide number of papers concerning swirling flows in engines and cyclone dust separators, where the vortex breakdown and precessing vortex core were observed and studied; examples are the experimental studies from Yazdabadi et al. (1994), where the approximate instantaneous position of the vortex core is determined, and Chao et al. (1991), where particular attention is given to velocity spectra of turbulent fluctuations. Among the theoretical papers concerning vortex breakdown, the one from Benjamin (1962) has given relevant insight into the possible physics of the phenomenon; further development of this theory or other interesting approaches have been proposed by many authors; in particular, an interesting interpretation of the spiral vortex breakdown as a nonlinear global mode and discussion concerning its characteristic precessing frequency has recently been presented by Ruith et al. (2003) and Gallaire et al. (2006), starting from numerical results obtained with DNS.

The work by Lucca-Negro and O'Doherty (2001) is an extensive and comprehensive review concerning the vortex instability and breakdown, while the recent review by Syred (2006) is mainly focused on the PVC phenomenon; finally, the textbook by Gupta et al. (1984) is a standard reference for the researchers working in this area.

The present work is concerned with the experimental analysis of an incompressible free swirling air jet, with particular regard to the so-called precessing vortex core instability. The experimental analysis of this flow was performed by means of LDV and particle image velocimetry. Processing of the large amount of data collected, and particularly the joint analysis of probability density functions and power spectral density functions of velocity components, led to a deeper understanding of the interaction between the PVC and the flow turbulence.

2 Problem definition

The flow considered in the present study is an incompressible free swirling jet of air at ambient pressure and temperature. The exhaust section is circular with radius R, and a cylindrical coordinate system is chosen with origin in its center. Coordinates for the axial, radial and azimuthal directions are indicated by z, r and θ and the corresponding velocity components are denoted by u, v and w, respectively.

The main feature of this jet is the large-scale vortical structure associated with the swirl. Then, the proper non-dimensional parameters characterizing this flow are obtained naturally in the derivation of the non-dimensional form of the vorticity equation. It is known that the vorticity equation can be expressed as follows:

$$\frac{\partial \boldsymbol{\omega}}{\partial t} + (\mathbf{v} \cdot \nabla)\boldsymbol{\omega} = v\Delta\boldsymbol{\omega} + (\boldsymbol{\omega} \cdot \nabla)\mathbf{v} \qquad (1)$$

where $\mathbf{v} = \{u,v,w\}$ is the velocity field, $\boldsymbol{\omega} = \nabla \times \mathbf{v}$ is the vorticity field and v is the kinematic viscosity of the fluid. In a swirling jet characterized by a reference value of vorticity Ω, a reference axial velocity U and a reference length $2R$, the proper reference time is $1/\Omega$. In the present work, the reference velocity U is obtained from the integral average of the axial velocity profile measured at the exhaust section, while the reference vorticity Ω is obtained from the integral average of the axial vorticity component, computed from the tangential velocity profile measured at the exhaust section. The non-dimensional form is obtained as follows (hats denote non-dimensional quantities):

$$\frac{\partial \hat{\boldsymbol{\omega}}}{\partial \hat{t}} + \frac{U}{2\Omega R}(\hat{\mathbf{v}} \cdot \hat{\nabla})\hat{\omega} = \frac{v}{4\Omega R^2}\hat{\Delta}\hat{\omega} + \frac{U}{2\Omega R}(\hat{\omega} \cdot \hat{\nabla})\hat{\mathbf{v}} \qquad (2)$$

Rearranging, one obtains:

$$\frac{\partial \hat{\boldsymbol{\omega}}}{\partial \hat{t}} + \frac{1}{G}\left[(\hat{\mathbf{v}} \cdot \hat{\nabla})\hat{\omega} - (\hat{\omega} \cdot \hat{\nabla})\hat{\mathbf{v}}\right] = \frac{1}{Re}\frac{1}{G}\hat{\Delta}\hat{\omega} \qquad (3)$$

where $G = \frac{2\Omega R}{U}$ is the swirl parameter and $Re = \frac{2UR}{v}$ is the Reynolds number. The swirl number S is commonly used in the literature concerning swirling jets to characterize the swirl intensity, and is defined by the following ratio, evaluated at the exhaust section (Gupta et al. 1984):

$$S = \frac{\int_0^{2\pi}\int_0^R (\rho uw + \rho\langle u'w'\rangle)r^2\,\mathrm{d}r\,\mathrm{d}\theta}{R\int_0^{2\pi}\int_0^R (\rho u^2 + \rho\langle u'^2\rangle + (p - p_\infty))r\,\mathrm{d}r\,\mathrm{d}\theta} \qquad (4)$$

where the primes denote velocity fluctuations, $< \cdot >$ is the averaging operator, ρ is the density and p denotes pressure. We prefer to use the swirl parameter G instead of the swirl number S because G is easily and completely defined with

the mean velocity profiles measured at the exhaust section, while the correct definition of S would require more complex measurements to obtain the turbulent stress and pressure terms; indeed, this inherent complication in the definition of S has led many authors to use simplified forms of the swirl number, which are hardly comparable. It is worth noting that the parameter G can be also interpreted as the ratio $(G = \tau_c/\tau_v)$ of a convective time scale $\tau_c = 2R/U$ to a vortex time scale $\tau_v = 1/\Omega$; both time scales are typical of the flow under consideration.

The PVC instability is experimentally investigated by means of LDV and PIV. In particular, the following conditions are considered:

- $G \approx 2.76$ and six values of Re, $24{,}400 < Re < 40{,}000$.
- $Re \approx 21{,}900$ and nine values of G, $1.46 < G < 4.48$.

3 Experimental apparatus and error estimation

The swirling flow is obtained with a swirl generator of axial-plus-tangential entry type; the swirl generator was the same of the one used in the swirl burner described, for example, in the work of Coghe et al. (2004). The swirl burner is characterized by the presence of a coaxial swirling air stream, around a central fuel injector. In the present work, this injector was moved below the throat of the burner of about five injector diameters from its original position, and was used for flow seeding with oil droplets.

The air flow, past the throat of the burner—which is circular with a diameter of 36 mm—flows through a converging nozzle; detailed drawing of the nozzle is reported in Fig. 1. The exhaust section of the nozzle has a diameter $2R = 24$ mm.

The total air flowrate and the swirl intensity are regulated by controlling the flowrates in both the axial and tangential entries and in the fuel gun. The flowrate regu-

Fig. 1 Schematic of the nozzle, measures in mm

lators are three Brooks Instrument thermal flowmeters, with a full scale of 200; 1,000 and 50 Nl/min, respectively. The error on the flowrate measurement is estimated around 1% of the full scale of each flowmeter.

Olive oil droplets were chosen as tracer particles in LDV and PIV measurements. The seeding system, very similar to classical medical aerosol apparata, generates oil droplets with an estimated diameter of about 1–2 μm. The maximum measurable frequency of the flow fluctuations, limited by the inertia of the tracer particles, was estimated to be around 12.7 kHz, and expresses the cut-off frequency at which the particles still follow the velocity fluctuations at 70% of their amplitude, assuming a first order, low pass filter response of particle motion (Albrecht et al. 2003). The actual temporal resolution of the LDV measurements depends on the validated rate of particles arrival in the probe volume. The Stokes number computed in the worst case is sufficiently less than one, thus the centrifugal effect on tracer particles can be considered negligible.

Laser Doppler velocimetry measurements were performed using a two component fiber optics LDV equipped with a Spectra Physics 'Stabilite 2017' Argon ion laser and a Bragg cell with 40 MHz frequency shift. All measurements were performed in back-scattering mode and the signal processing was performed with two Burst Spectrum Analysers (BSA-Dantec). The size of the probe volume $(0.09 \times 0.09 \times 0.84$ mm^3 in size, based on the e^{-2} intensity) was chosen to compromise spatial and temporal resolutions needed to correctly measure statistical quantities and spectra. The diameter of 0.09 mm was estimated small enough to avoid significant errors even in the regions of high spatial velocity gradients (≈ 3 m/s mm). It also enables correct resolution of the characteristic frequencies of the PVC (<1 kHz) (Albrecht et al. 2003). The overall probe volume dimensions and the number density of the seeding particles allowed to obtain typical mean data rates larger than 5 kHz. Analysis of the LDV data was performed with in-house routines, and statistics and probability density functions were computed employing a correction for the transit time to reduce the velocity bias error. All the power spectral density functions were obtained with a Sample and Hold and resampling method (Nobach et al. 1998), and averaged over at least 30 data records. Following Albrecht et al. (2003), an estimation of the statistical error on the mean and r.m.s. values should be based on the number N of statistically independent samples; this number can be estimated by the relationship $N = \frac{T}{2T_i}$ where T is the time interval required to acquire each block of data, and T_i is an integral time scale of the phenomenon which can be estimated from the convective time scale $T_i \approx 2R/U \approx 1$ ms. Typically, the samples acquired at each measurement point were 160,000 with a mean data rate of 5 kHz and so $T \approx 30$ s. Then, the
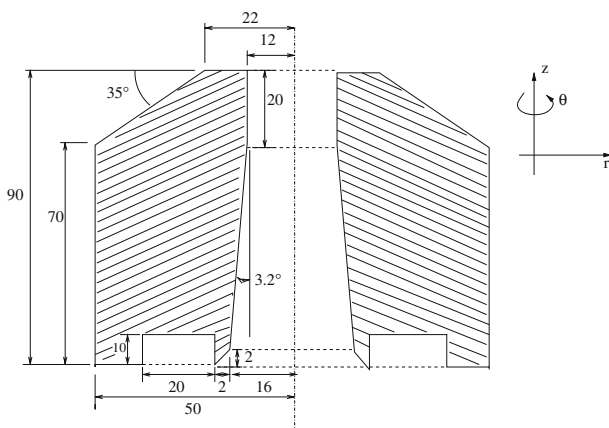
number of independent samples is $N \approx 15{,}000$; based on this number, both the relative error on the mean value and on the r.m.s. are estimated to be less than 2%.

Particle image velocimetry measurements were performed using a double pulsed Nd:YAG laser by Quanta Systems, operating at 532 nm, with pulse energy of 200 mJ/pulse. Images were acquired with a Dantec HiSense PIV Camera, and processed with Dantec PIV FlowSoftware. The spatial resolution of PIV measurements in the plane of the laser sheet is estimated to be about 1 mm, and the spatial resolution in the direction normal to this plane is estimated from the average thickness of the laser sheet, which is about 1 mm; the spatial resolution of the PIV instrument and particularly the thickness of the probe volume was dictated by considerations on the possible loss of particle pairs due to the high transverse velocity component. PIV measurements were performed at the same vertical location of LDV measurements, in order to obtain cross flow velocity fields, i.e., velocity fields on a plane normal to the nozzle axis; data acquisition was performed at the frequency of 1 Hz, with a time interval of 10 μs between the two laser pulses. The statistical error relative to the mean value of the velocity is estimated to be less than 6%, based on the 200 couples of images acquired at each experimental condition.

An Isel Automation traversing system was used to traverse the LDV system and the PIV camera; the spatial resolution of this system is 0.1 mm.

The temperature of the air was measured at the inlet of the air line with a PT 100 platinum thermistor, and remained at 18.0 ± 0.5°C during the whole measurement session; thus experimental results can be considered not to be affected by an error due to temperature drift.

More details about the experimental setup can be found in Martinelli (2005).

4 Results

4.1 Results with constant G

Mean velocity and standard deviation profiles were obtained from LDV measurements and are reported for both velocity components in Fig. 2, parametrized with Re; the spatial resolution in radial direction was 1 mm, in accordance with the length of the probe volume. All results are coherent with data reported in literature.

Mean axial velocity profiles indicate that the hypothesis of plug flow at the exhaust section is very far from reality. The average axial flow shows a region of downward velocity, that indicates the presence of an important recirculation zone (well known in literature as central toroidal recirculation zone - CTRZ) due to the adverse pressure

gradient in axial direction; this feature is confirmed by similar measurements (not reported here) performed at $z/2R \approx 0.6$ from the exhaust section, where an increase in the width of the recirculation zone is also observed. Far from the nozzle axis, the magnitude of the axial component increases strongly, and peaks are found at about $r \approx R$ for all the Re considered. Mean tangential velocity profiles indicate that the hypothesis of solid body rotating core is justified at least in the inner core, where the tangential velocity increases almost linearly from $r/R = 0$ to $r/R \approx 0.5$.

Standard deviation profiles indicate that very strong velocity fluctuations are present; in particular, the values of the r.m.s. may become comparable with those of the mean velocity. High values of the r.m.s. of the tangential component for $r = 0$ are normally explained as an effect due to the presence of the precessing vortex core and not representative of the true turbulence (Heitor and Whitelaw 1986).

Power spectral density functions (PSD) of the velocity components were evaluated for each measurement point of the velocity profiles. For the sake of brevity, two representative PSDs—normalized with the variance—are reported in Fig. 3a, for both velocity components, showing the presence of a strong peak corresponding to the same characteristic frequency; a similar discrete frequency in the spectrum was observed in highly swirling flows in a gas turbine combustor and attributed to a precessing vortex core (McGuirk and Palma 1995b). In Fig. 3b, the corresponding normalized probability density functions (PDF) are shown. It is interesting to note the symmetric bimodality characterizing the PDF of the tangential component; this feature is typical of all the PDFs of the tangential component at $r = 0$. Bimodality of PDFs was also reported in the work by McGuirk and Palma (1995b), but was due to a different kind of instability.

In Fig. 4 it is shown that an almost linear relation exists between the peak frequency and Re; this is a typical feature of the PVC instability (Gupta et al. 1984), and further confirmation of the presence of the precessing vortex core will be presented in the following of the paper. The curve represents the best linear fitting in the least-squares sense; the corresponding Strouhal number is $St = \frac{f_{\mathrm{PVC}}2R}{U} \approx 0.78$ and the ratio $f_{\mathrm{PVC}}/\Omega = St/G \approx 0.28$. Analysis (not reported here) of all the power spectral density functions computed confirms that the peak frequency does not vary along the radius nor along the axis, for a given Re.

The joint analysis of the PSDs and PDFs of both velocity components can give a significant insight in the interpretation of vortex precession. The features of the spectra in Fig. 3a suggest that a generic component of the velocity at a fixed position and as a function of time may be decomposed as follows:
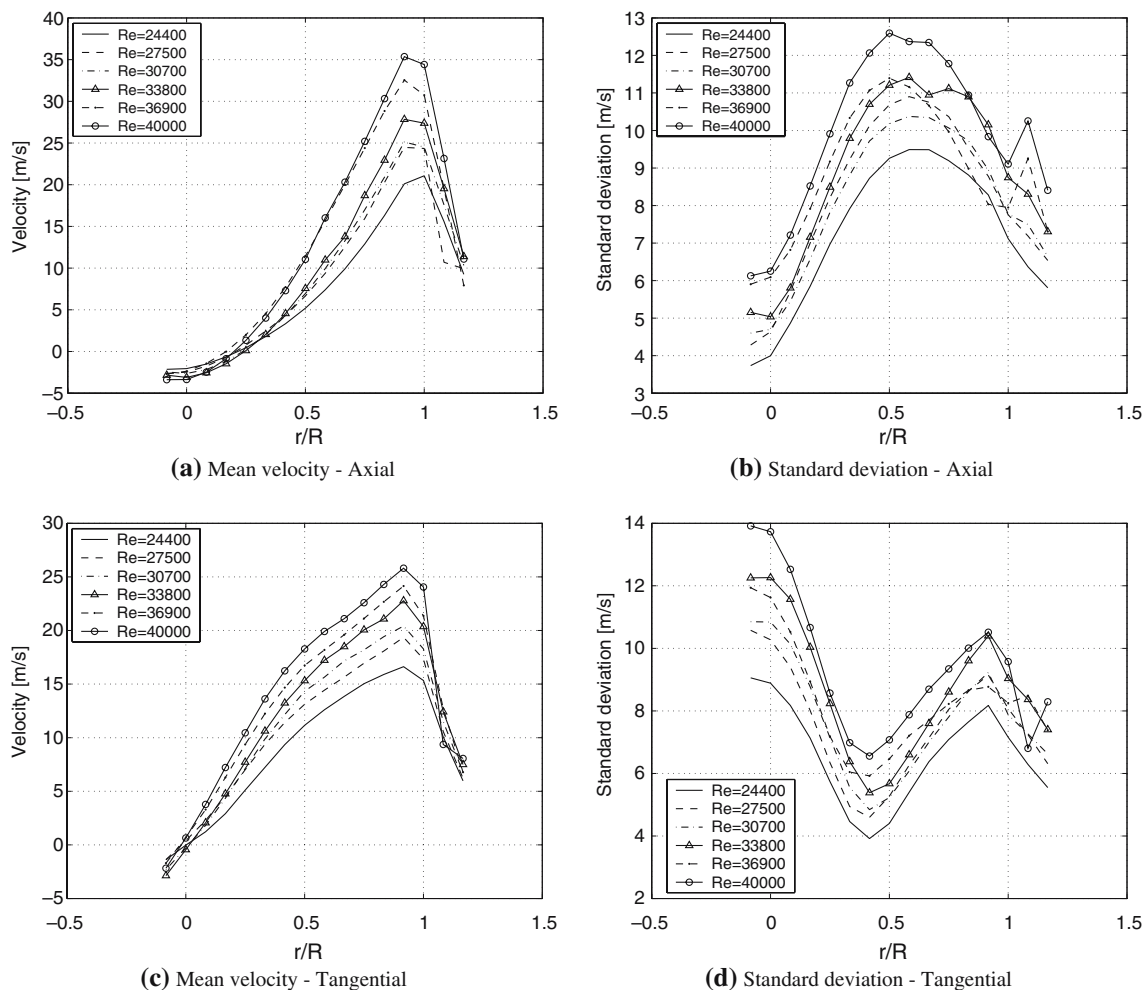
(a) Mean velocity - Axial

(b) Standard deviation - Axial

(c) Mean velocity - Tangential

(d) Standard deviation - Tangential

Fig. 2 Mean velocity and standard deviation profiles, parametrized with $Re - G \approx 2.76$

$$u(t) = \underbrace{A\sin(2\pi f_{\text{PVC}}t)}_{x(t)} + \underbrace{u'(t) + \mu_y}_{y(t)}$$

where the term $x(t)$ represents the periodic oscillation due to the PVC and $y(t)$ represents the random background turbulence, whose fluctuating part $u'(t)$ around the mean value μ_y is characterized by a standard deviation σ_y. This decomposition allows to determine an analytical expression for the PDF of the term $u(t)$ (see the Appendix for the derivation and discussion):

$$p_u(u) = \frac{1}{\sqrt{2\pi}} \frac{1}{\pi \sigma_y} \int_{-\infty}^{+\infty} \frac{1}{\sqrt{A^2 - x^2}} e^{-\frac{(u-x-\mu_y)^2}{2\sigma_y^2}} \, \mathrm{d}x$$

This analytical PDF (hereinafter called model PDF) is completely defined given the three parameters A, σ_y and μ_y. Assuming that the proposed decomposition captures the relevant flow physics, the analytical PDF must be representative of the experimental ones; consequently,

interpolation of the experimental PDFs of the u and w components with the model PDF leads to the determination of the three parameters A, σ_y and μ_y, properly separating the turbulence term from the large scale velocity fluctuation due to vortex precession. All the experimental PDFs obtained at $r = 0$ at the exhaust section were interpolated in the least-squares sense with the model PDF proposed above, and an example of interpolation is given in Fig. 5.

The interpolation process resulted in very good approximations of the experimental PDFs by the model PDF; the values of the correlation coefficient resulted higher than 0.98 in all cases. The parameters A, σ_y and μ_y calculated at the exhaust section at $r = 0$ are shown in Fig. 6 as functions of Re, for both velocity components; moreover, the standard deviation computed from raw data (St.d.) is reported for comparison purposes. The mean value of the tangential component is zero for symmetry considerations, while the mean value of the axial component tends to decrease, as it is expected from the results
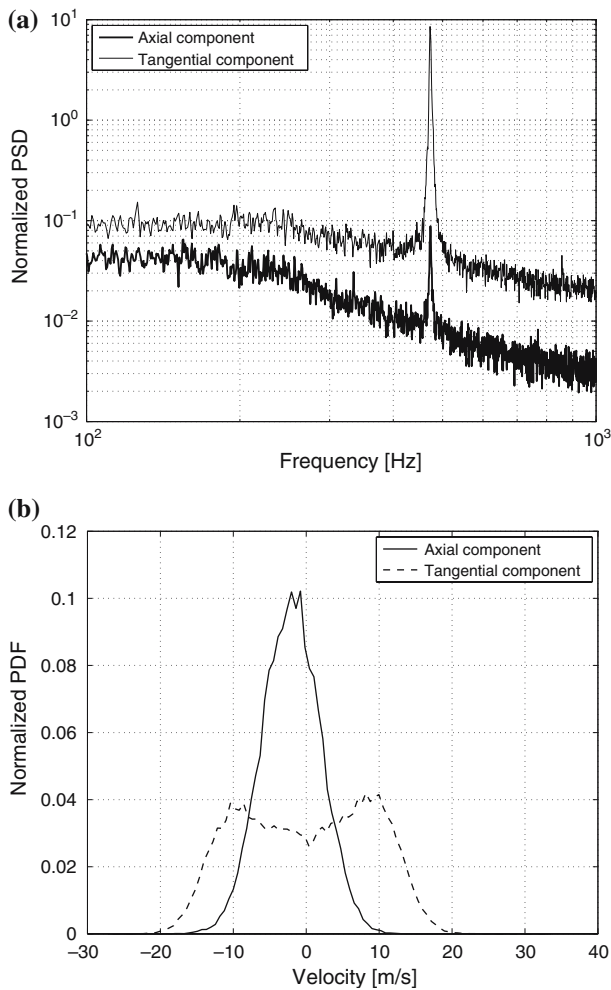
Fig. 5 Example of interpolation of a probability density function $Re \approx 24400$, $G \approx 2.76$

Fig. 3 **a** Example of PSD for the axial (*lower*) and tangential (*upper*) velocity component, at $r = 0$. **b** Example of PDF for the axial (*solid*) and tangential (*dashed*) velocity component, at $r = 0$. Both figures refer to a condition of $Re \approx 24400$, $G \approx 2.76$
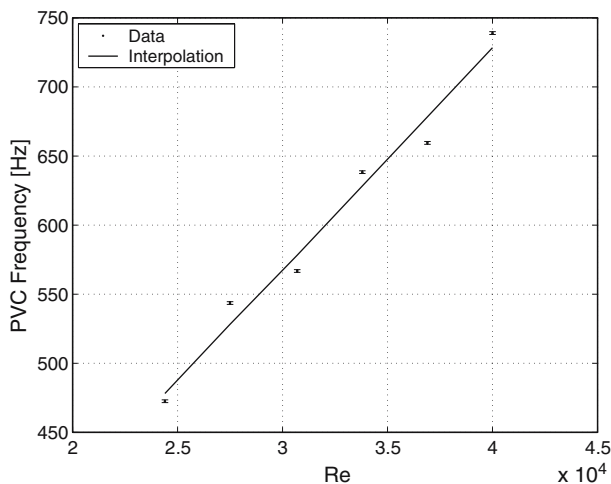

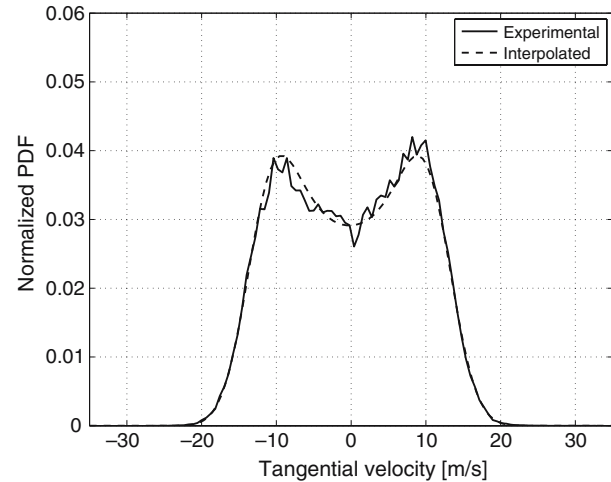**Fig. 4** Linear dependence between peak frequency and Re – $G \approx 2.76$

reported in Fig. 2. The St.d. increases with Re as well as the amplitude A of the periodic term due to the PVC; however, the true standard deviation σ_y, representative of the true turbulence intensity, increases weakly. It is apparent, in particular for the tangential component, that the strong increase of the St.d. can be properly interpreted as an effect of the PVC.

Average PIV velocity maps are in good agreement with LDV results, confirming that the present PIV measurements do not suffer from errors due to the velocity component perpendicular to the laser sheet. It was possible to obtain high quality instantaneous maps, that confirmed the precession motion of the vortex center. The overall appearance of the instantaneous velocity fields does not vary with Re; an example of instantaneous velocity field at the exhaust is reported in Fig. 7, where it is compared with a typical average velocity field in the same conditions. The validation rate (according to standard validation criterion of PIV data, i.e., peak ratio validation) is quite high in the region of interest. It is evident that the instantaneous velocity field does not show the symmetry of the average one; moreover, it is possible to easily localize the vortex core, since the core structure is evident.

In order to localize the instantaneous position of the vortex center, the method proposed in Grosjean et al. (1997) was implemented. The heart of this method consists in the determination of the vortex center as the location of the maximum of a properly defined normalized angular momentum computed from each instantaneous velocity field. Due to PIV resolution, the instantaneous position of the vortex center is determined with an accuracy of about 1 mm. Data analysis led to the approximate determination of a cloud of points, representative of the trajectory of the vortex center in the plane of the laser sheet; these instan-
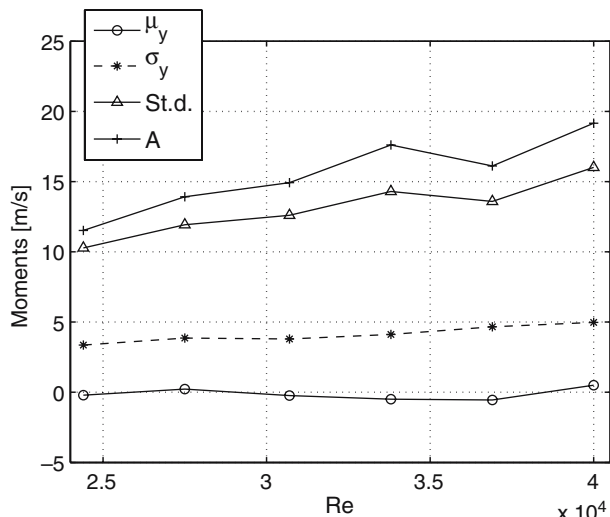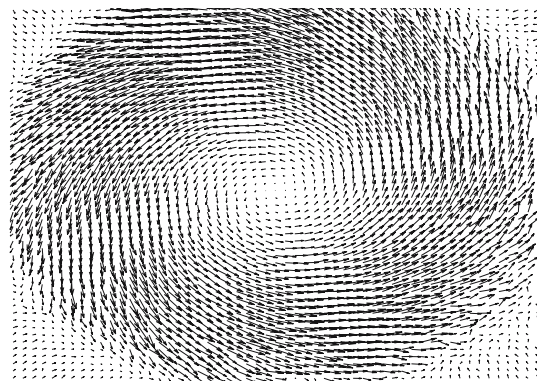
(a) Tangential component
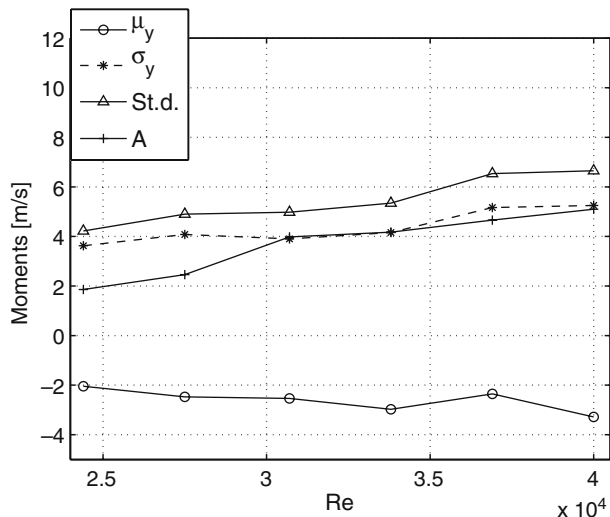
(b) Axial component

Fig. 6 Interpolation of the PDFs: relevant parameters versus *Re*. Results for $G \approx 2.76$, $r = 0$

(a) Average velocity field

(b) Instantaneous velocity field

Fig. 7 Comparison between average and instantaneous velocity fields at the exhaust. **a** The vertical dimension should be enlarged to become equal to the horizontal one to show a circular pattern; **b** The vertical dimension should be enlarged to become equal to the horizontal one to show a circular pattern
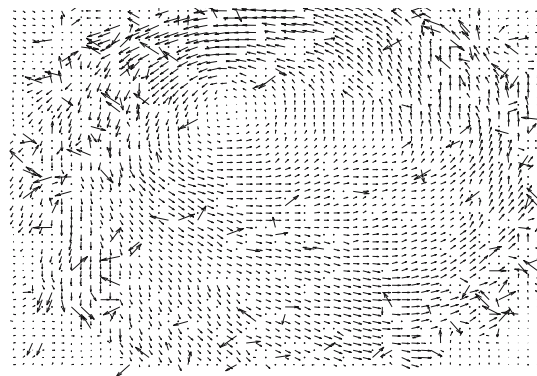
taneous positions were used to determine a circular path, centered at the position of the nozzle axis and having radius R_p, that approximates in the least squares sense the trajectory of the vortex core. In Fig. 8 it is shown that the ratio of the interpolating radius to the exhaust radius R_p/R is almost constant with *Re*; this indicates that the size of the precessing path is quite independent of *Re*, in the range of *Re* considered. In the present experimental conditions it is also found that the PVC precesses, on average, outside the boundary of the CTRZ.

4.2 Results with constant *Re*

The range of swirl parameters *G* considered in the complementary analysis at constant $Re \approx 21{,}900$ at the exhaust

section was chosen with the purpose of studying the inception of the vortex breakdown and settlement of PVC.

Velocity profiles obtained from LDV data are reported in Fig. 9, parametrized with respect to *G*: only five cases are reported for the ease of reading figures. Inspection of the axial velocity profiles in Fig. 9 shows immediately that a range of values around $G = 2.34$ corresponds to a critical situation; in fact, for $G \leq 1.46$, the mean axial velocity profiles are monotonically decreasing along the radius, while for $G \geq 3.10$ a central recirculation zone appears; this may be considered an indication of the insurgence of the vortex breakdown observed in swirling jets (Lucca-Negro and O'Doherty (2001), see also Ruith et al. 2003). Coherently, standard deviation profiles show that $G = 2.34$ corresponds to a critical situation between two different flow conditions. The modifications of tangential velocity profiles with *G* are less evident; however, it is shown that the size of the solid-body rotation core increases monotonically with *G*. Also, standard deviation tends to increase with *G* in each measurement point. The value $\tilde{G} = 2.34$
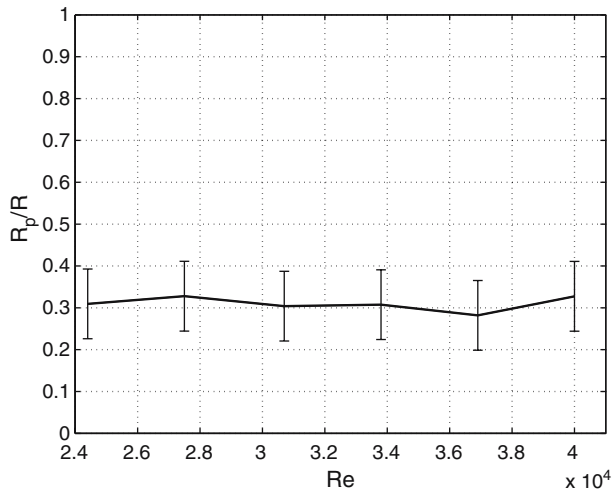
Fig. 8 Ratio of the average precessing radius on the exhaust radius (R_p/R) versus Re, at $G \approx 2.76$

will be called hereinafter critical swirl parameter; accordingly, the flow regimes for $G < \tilde{G}$ will be called supercritical, otherwise subcritical. This nomenclature is coherent to

that chosen by Benjamin (1962) to describe the capability of a swirling jet to sustain standing perturbation waves (see also Lucca-Negro and O'Doherty (2001) and Ruith et al. 2003).

Probability density functions and power spectral density functions were computed from the data collected, as reported in the previous section. Joint analysis of PDFs and PSDs for both components, as measured at $r = 0$ and for three significant values of G, is reported in Figs. 10 and 11. In supercritical conditions, velocity spectra of both components do not show any particular feature, as well as the corresponding PDFs, that are approximately gaussian. In critical conditions, the shape of velocity spectra changes and, for the tangential component, a peak appears in the vicinity of the precessing frequency. The PDF of the tangential component appears almost gaussian and symmetric, while the one of the axial component shows an asymmetric bimodality due to the formation of an unsteady axial recirculation zone: this is the onset of the instability. In subcritical conditions, a well defined peak appears in the velocity spectra of both components; the tangential PDF
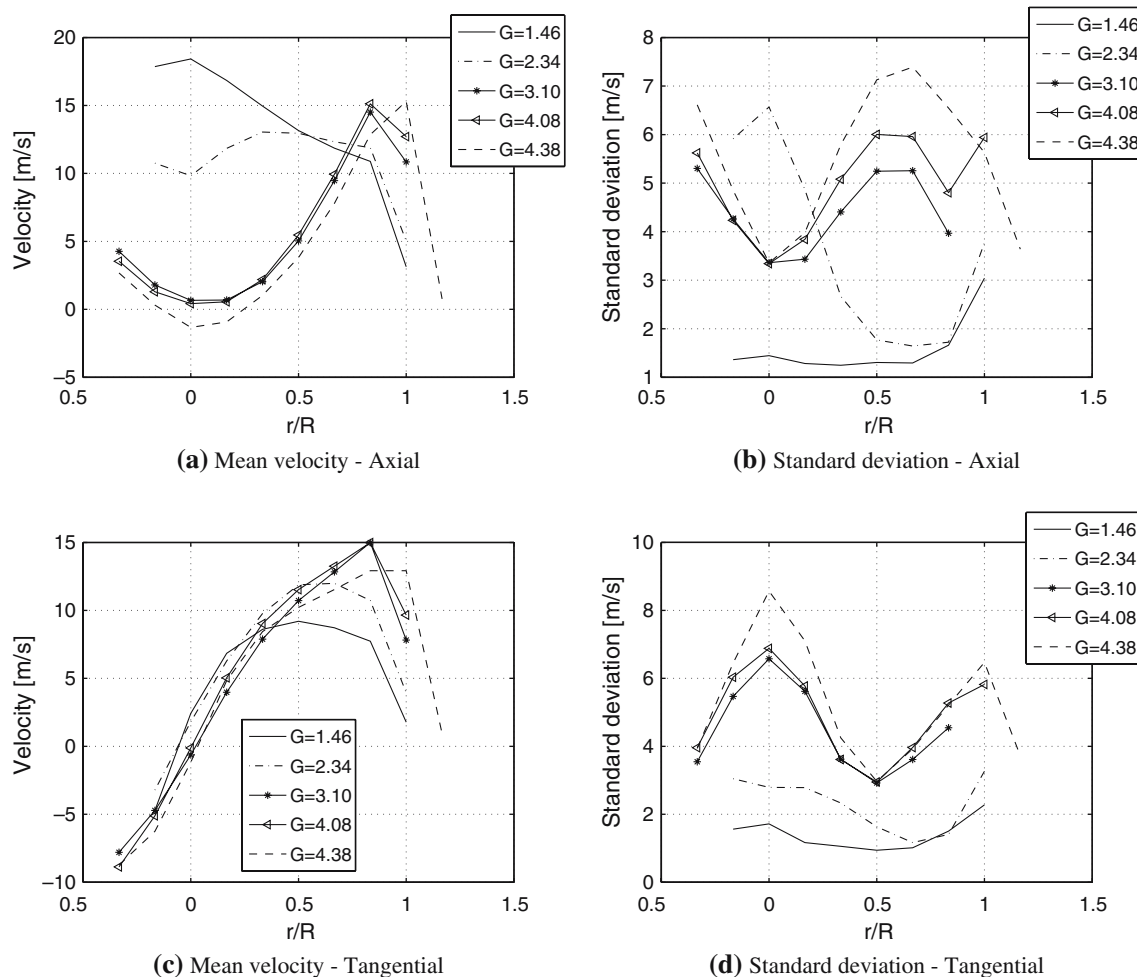

(a) Mean velocity - Axial

(b) Standard deviation - Axial

(c) Mean velocity - Tangential

(d) Standard deviation - Tangential

Fig. 9 Mean velocity and standard deviation profiles, parametrized with $G - Re \approx 21{,}900$
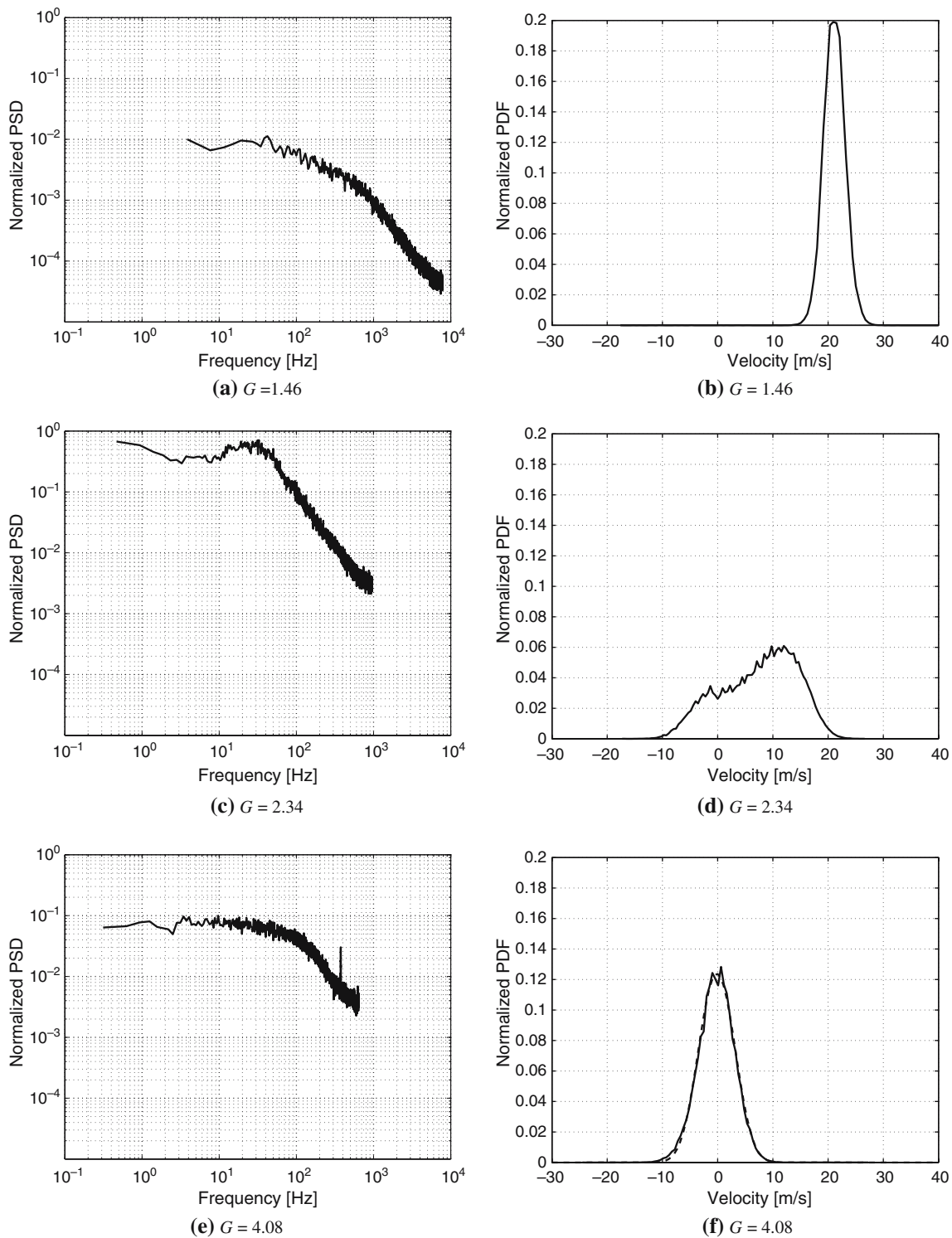
Fig. 10 PSDs and PDFs of the axial component, measured at $r = 0 -$ $Re \approx 21{,}900$. The parametrization with respect to G shows the transition from supercritical to subcritical conditions, $G \approx 2.34$ being the critical swirl parameter. The maximum frequency of the PSDs in **c** and **e** is lower than in **a** because of a lower mean data rate. In **f** the model PDF (*dashed line*) is plotted with the experimental curve (*solid line*)

shows symmetric bimodality, while the axial one resembles a gaussian PDF. The PVC has settled and the axial recirculation zone is stable, on average.

Proper interpolation of the experimental PDFs was performed as described in the previous section. As the model PDF requires a periodic term in the velocity signal,
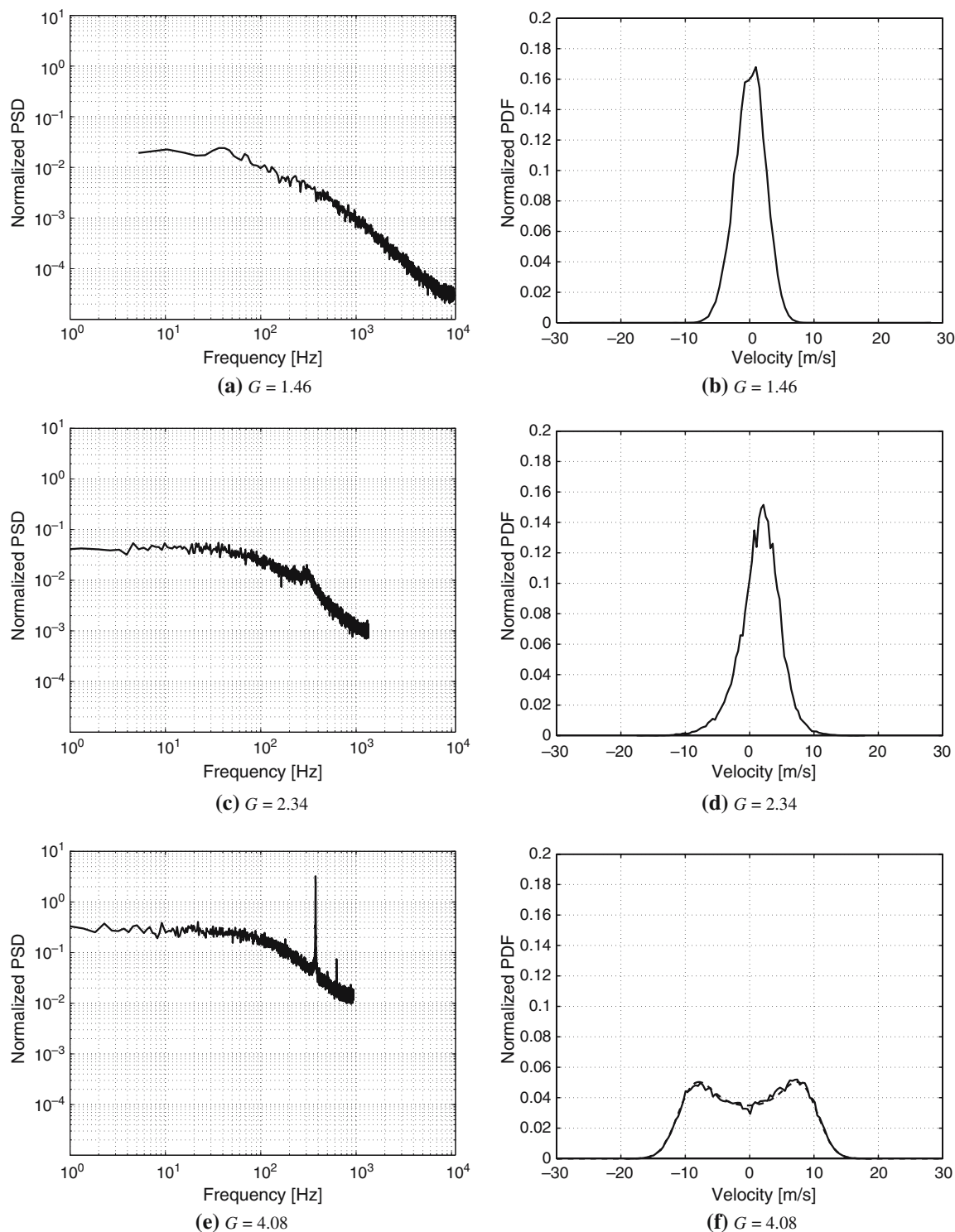
Fig. 11 PSDs and PDFs of the tangential component, measured at $r = 0 - Re \approx 21{,}900$. The parametrization with respect to G shows the transition from supercritical to subcritical conditions, $G \approx 2.34$ being the critical swirl parameter. The maximum frequency of the

PSDs in **c** and **e** is lower than in **a** because of a lower mean data rate. In **f** the model PDF (*dashed line*) is plotted with the experimental curve (*solid line*)

interpolation results are referred to subcritical conditions only, and are shown in Fig. 12 for both velocity components at $r = 0$. Considering the tangential component, it is

shown that the amplitude of the fluctuation associated to the PVC increases with the swirl parameter G, as well as the St.d. term; on the contrary, the true turbulence intensity

appears to be independent from G, as it is expected since the Reynolds number is kept fixed. The mean value is about zero for symmetry considerations. Results for the axial component show that for this value of Re the influence of the PVC on the standard deviation computed from raw data (St.d.) is very weak; as a consequence, it is not possible to evidence any particular trend with G of the parameters A and σ_y. This result is in agreement with the fact (also shown in Fig. 6) that the effect of the PVC on the tangential component is much more evident than the effect on the axial one. Finally, due to the formation of the CTRZ, the mean axial velocity on the axis at the exhaust section decreases with G.

Particle image velocimetry measurements were performed in the same conditions, and instantaneous velocity fields were analyzed as described in the previous section. Results do not show any particular trend with G of

(a) Tangential component

(b) Axial component

Fig. 12 Interpolation of the PDFs: relevant parameters versus G. Results for $Re \approx 21{,}900$, $r = 0$

the radius interpolating the precessing path of the vortex center.

4.3 Discussion

The analysis of the experimental results at constant G shows that, when the instability has settled, the qualitative behavior of the velocity and r.m.s. radial profiles does not change with Re, as it is expected for an high Reynolds number turbulent flow. The radial extent of the axial recirculation zone is almost constant and the maximum negative value of the axial velocity (on the nozzle axis at the exhaust section) increases with Re. The analysis of the spectral content of the velocity fluctuations confirms the almost linear relation between the precessing frequency and the Reynolds number (Fig. 4). The interpolation of the PDFs has shown that the amplitude A of the periodic component is dependent on Re (Fig. 6), and that the increase of true turbulence intensity with Re is weaker than the increase of the standard deviation computed from raw data. Finally, the analysis of instantaneous PIV maps has shown that the radius of the average trajectory of the instantaneous vortex center is almost independent from Re.

Analysis at constant Re has shown that the inception and settlement of the instability is a three-stage process. This result is evident from the large modifications of the velocity profiles from supercritical to subcritical conditions. Joint analysis of the velocity PDFs and power spectra as functions of G confirms that the settlement of the PVC coincides with the formation of the axial recirculation zone (Lucca-Negro and O'Doherty 2001). Proper analysis of the PDFs has shown that the amplitude of the fluctuating term due to PVC is a function of the swirl parameter G, while the true turbulence intensity is independent of G.

The results reported above allow to argue the following properties of the precessing vortex core:

- The amplitude A of the periodic component due to vortex precession is a function of Re and G.
- The true turbulence intensity, represented by σ_y, appears to be a function of Re and independent of G.

These considerations suggest that the PVC does not interact strongly with the small scale turbulence, at least for the range of explored conditions; this fact is coherent with the observation that the peak in the velocity spectra lies in the inertial range.

The separation of the coherent flow pulsations of the PVC from true turbulence has relevant consequences from the point of view of numerical simulations of this kind of flow; in particular, as already noticed by McGuirk and Palma (1995a), numerical approaches based on steady-state formulations of the govering equations fail in capturing the physics of the flow. In the present case of non-stationary
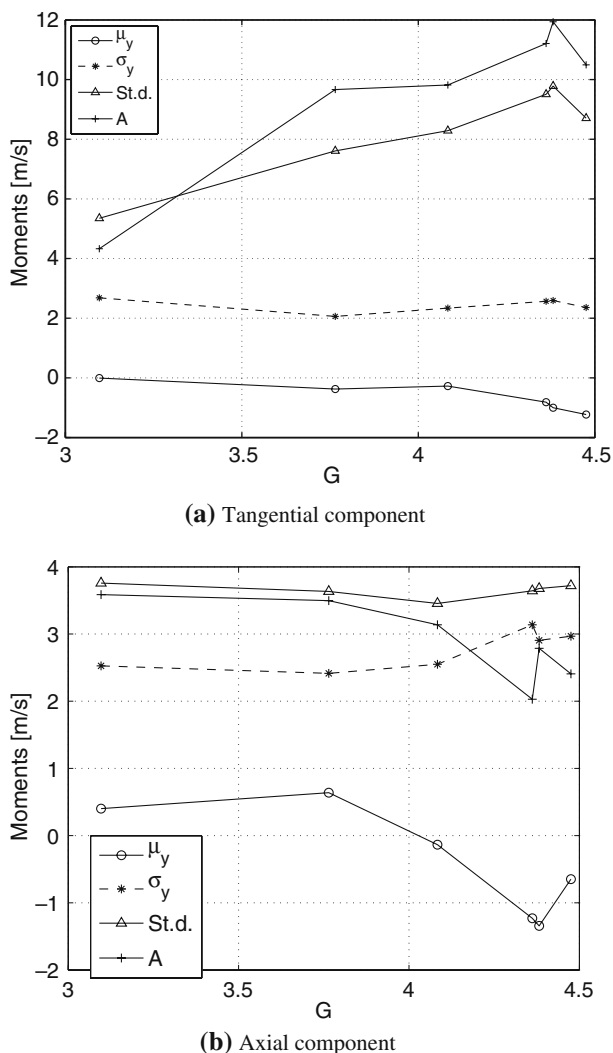
flow there is the need to decompose the total fluctuation energy into a periodic part and a random part. Such partitioning has been obtained by Grosjean et al. (1997) by combining LDV and PIV measurements with an original approach which cannot be used in strongly turbulent swirling flows. The approach shown in the present work allows quantitative partitioning of fluctuation energy only by a joint analysis of the PDFs and power spectra of the velocity data obtained from point LDV measurements, and provides meaningful results even in a strongly turbulent swirling jet.

5 Conclusions

An experimental analysis of the precessing vortex core instability was performed on a free swirling jet using LDV and PIV. The two parametric studies of the phenomenon (at constant swirl parameter G and at constant Reynolds number Re) have shown the trends of the relevant variables characterizing the flowfield. Analyses of the velocity profiles as well as power spectral density functions and probability density functions were performed; proper decomposition of the velocity was proposed and was shown to be significant in the analysis of the PDFs obtained experimentally. It was found that the true turbulence intensity, associated with the small scale flow turbulence, can be separated from the periodic fluctuations due to precession and is independent of G. Moreover, it was shown that the main feature of the PVC, i.e., the amplitude of the corresponding periodic fluctuation, is dependent on both Re and G. The characteristic size of the precession region was shown to be almost independent of Re.

6 Appendix: derivation of the model PDF

Let us assume that the velocity field under consideration is statistically stationary, and that the phenomenon is ergodic. Moreover, let us assume that a velocity component in a generic point in the flowfield can be decomposed in three contributions: a mean value μ, a term due to the periodicity of the PVC and a term due to turbulence. Thus, in a generic experiment k, the velocity signal v_k as a function of time can be written as follows:

$$v_k(t) = \underbrace{A\sin(2\pi f_{PVC}t + \theta_k)}_{x_k(t)} + \underbrace{v_k'(t) + \mu_y}_{y_k(t)}$$

A Gaussian probability density function for the turbulent term is assumed:

$$p_y(y) = \frac{1}{\sqrt{2\pi}\sigma_y}e^{-\frac{(y-\mu_y)^2}{2\sigma_y^2}} \tag{5}$$

and it is completely defined by its mean value and standard deviation μ_y and σ_y, obtained by ensemble averaging at each time instant on the set of phase-locked experiments.

θ_k denotes the initial phase of the PVC signal in the generic experiment k and is assumed to be uniformly distributed between 0 and 2π; as a consequence, the periodic term can be regarded as a random variable itself. Under this assumption, the probability density function of the term x can be expressed as follows:

$$p_x(x) = \frac{1}{\pi\sqrt{A^2 - x^2}} \quad \text{for } -A < x < A$$
$$p_x(x) = 0 \quad \text{otherwise} \tag{6}$$

Let us assume that the two velocity terms x and y can be considered statistically independent. This allows for the
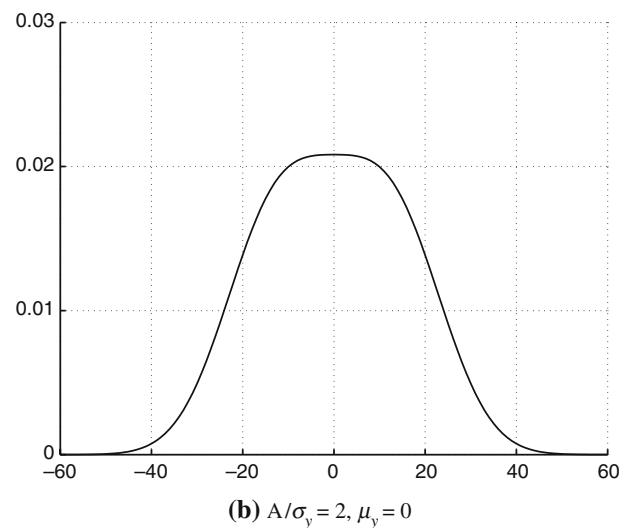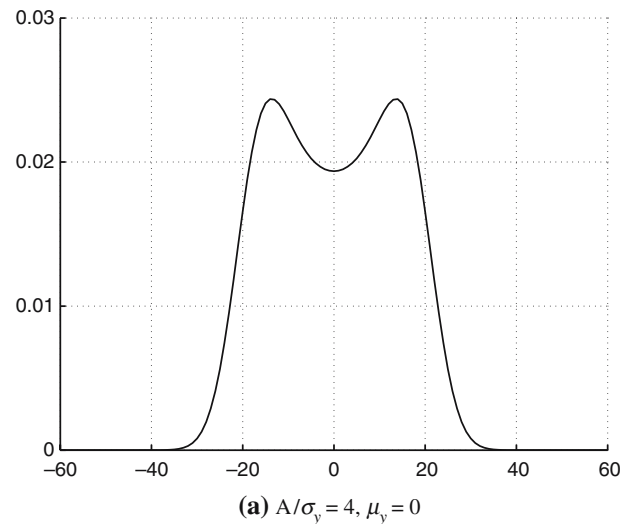

(a) A/σ_y = 4, μ_y = 0

(b) A/σ_y = 2, μ_y = 0

Fig. 13 Probability density function $p_v(v)$ for two different values of A/σ_y; when the ratio A/σ_y decreases, the PDF tends to resemble a Gaussian

joint PDF function $p(x, y)$ to be expressed as a product of the single probability density functions $p_x(x)$ and $p_y(y)$. Then, the probability density function $p_v(v)$ of the sum $v = x + y$ is readily obtained from (Bendat and Piersol 1986):

$$p_v(v) = \int_{-\infty}^{+\infty} p_x(x) p_y(v - x) \mathrm{d}x \qquad (7)$$

and then

$$p_v(v) = \frac{1}{\sqrt{2\pi}} \frac{1}{\pi \sigma_y} \int_{-\infty}^{+\infty} \frac{1}{\sqrt{A^2 - x^2}} e^{-\frac{(v - x - \mu_y)^2}{2\sigma_y^2}} \mathrm{d}x \qquad (8)$$

This is the general expression of the probability density function of the random variable v; it is a symmetric function by construction and is uniquely defined by the parameters A, σ_y and μ_y. This integral cannot be evaluated analytically and must be computed numerically; examples, reported in Fig. 13, are both computed for a value of $\mu_y = 0$, and values of $A/\sigma_y = 4$ and $A/\sigma_y = 2$, respectively. It is worth noting that when the ratio A/σ_y decreases, the model PDF resembles a Gaussian one.

References

Akhmetov D, Nikulin V, Petrov V (2004) Experimental study of self-oscillations developing in a swirling-jet flow. Fluid Dyn 39(3):406–413

Albrecht H, Borys M, Damaschke N, Tropea C (2003) Laser Doppler and phase Doppler measurement techniques. Springer, Berlin Heidelberg New York

Bendat J, Piersol A (1986) Random data: analysis and measurement procedures. Wiley, New York

Benjamin TB (1962) Theory of the vortex breakdown phenomenon. J Fluid Mech 14:593–629

Billant P, Chomaz J, Huerre P (1998) Experimental study of vortex breakdown in swirling jets. J Fluid Mech 376:183–219

Cala CE, Fernandes EC, Heitor MV, Shtork SI (2006) Coherent structures in unsteady swirling jet flow. Exp Fluids 40:267–276

Cassidy J, Falvey H (1970) Observations of unsteady flow arising after vortex breakdown. J Fluid Mech 41:727–736

Chanaud R (1965) Observations of oscillatory motion in certain swirling flows. J Fluid Mech 21:111–127

Chao Y, Leu J, Hung Y, Lin C (1991) Downstream boundary effects on the spectral characteristics of a swirling flowfield. Exp Fluids 10(6):341–348

Coghe A, Solero G, Scribano G (2004) Recirculation phenomena in a natural gas swirl combustor. Exp Therm Fluid Sci 28:709–714

Dellenback P, Metzger D, Neitzel G (1988) Measurements in turbulent swirling flow through an abrupt axisymmetric expansion. AIAA J 26(6):669–681

Gallaire F, Ruith M, Meiburg E, Chomaz JM, Huerre P (2006) Spiral vortex breakdown as a global mode. J Fluid Mech 549:71–80

Garg AK, Leibovich S (1979) Spectral characteristics of vortex breakdown flowfields. Phys Fluids 22:2053–2064

Grosjean N, Graftieaux L, Michard M, Hubner W, Tropea C, Volkert J (1997) Combining LDA and PIV for turbulence measurements in unsteady swirling flows. Meas Sci Technol 8:1523–1532

Gupta A, Lilley D, Syred N (1984) Swirl flows. Abacus Press, London

Harvey J (1962) Some observations of the vortex breakdown phenomenon. J Fluid Mech 14:585–592

Heitor MV, Whitelaw JH (1986) Velocity, temperature, and species characteristics of the flow in a gas-turbine combustor. Combust Flame 64:1–32

Lucca-Negro O, O'Doherty T (2001) Vortex breakdown: a review. Prog Energy Comb Sci 27(4):431–481

Martinelli F (2005) Analysis of the precessing vortex core instability in a free swirling jet. Master Thesis, Politecnico di Milano

McGuirk JJ, Palma JMLM (1995a) Experimental investigation of the flow inside a water model of a gas turbine combustor: part 1—mean and turbulent flowfield. J Fluids Eng 117:450–458

McGuirk JJ, Palma JMLM (1995b) Experimental investigation of the flow inside a water model of a gas turbine combustor: part 2—higher order moments and flow visualization. J Fluids Eng 117:459–467

Nobach H, Muller E, Tropea C (1998) Efficient estimation of power spectral density from laser Doppler anemometer data. Exp Fluids 24(5–6):499–509

Novak F, Sarpkaya T (2000) Turbulent vortex breakdown at high Reynolds numbers. AIAA J 38(5):825–834

Ruith MR, Chen P, Meiburg E, Maxworthy T (2003) Three-dimensional vortex breakdown in swirling jets and wakes: direct numerical simulation. J Fluid Mech 486:331–378

Sarpkaya T (1971) On stationary and travelling vortex breakdowns. J Fluid Mech 45(3):545–559

Syred N (2006) A review of oscillation mechanisms and the role of the precessing vortex core (PVC) in swirl combustion systems. Prog Energy Comb Sci 32:93–161

Wunenburger R, Andreotti B, Petitjeans P (1999) Influence of precession on velocity measurements in a strong laboratory vortex. Exp Fluids 27:181–188

Yazdabadi P, Griffiths A, Syred N (1994) Characterization of the PVC phenomena in the exhaust of a cyclone dust separator. Exp Fluids 17(1–2):84–95